Organic–Inorganic Hybrid Composites

Chemically Exfoliated MoS$_2$ as Near-Infrared Photothermal Agents**

Stanley S. Chou,* Bryan Kaehr,* Jaemyung Kim, Brian M. Foley, Mrinmoy De, Patrick E. Hopkins, Jiaxing Huang, C. Jeffrey Brinker, and Vinayak P. Dravid

The near-infrared (NIR) window refers to a range of wavelengths (700–1300 nm) in which biological tissues are highly transparent.[1] Consequently, biological imaging and therapy modalities employ light at these wavelengths for the monitoring[1] and triggering[2] of biological events in vitro and in vivo. For instance, photothermal ablation takes advantage of NIR absorbing materials for transducing light into heat.[2] The resultant thermal energy can be used for a number of applications, such as tissue ablation and drug release. Despite the intense interest in NIR photothermal agents, their development has suffered from considerable challenges. In particular, few nanomaterials display the requisite absorption profiles required for NIR photothermal transduction.

The initial development of NIR photothermal agents largely focused on anisotropic gold particles[3] such as nanorods,[2] nanocages,[4] and nanostars.[5] These shapes serve as local plasmon antennas for NIR absorbance, but they are encumbered by complicated syntheses. More importantly, because of the non-equilibrium morphologies, anisotropic gold nanostructures inevitably tend to evolve into spheres upon heating.[5]

Consequently, researchers have begun to investigate the NIR photothermal properties of graphene derivatives such as graphene oxide (GO)[6] and reduced graphene oxide (rGO).[7] The exceptional surface-area-to-mass ratio of these two-dimensional (2D) materials makes them promising photothermal candidates that can be loaded with high cargo concentrations. Previously graphene,[8] rGO,[9] and MoS$_2$[10] among others[11] have been explored for their use as photodectors. However, a NIR photocurrent response for mechanically exfoliated MoS$_2$ phototransistors was negligible.[10] Additionally, the efficacy of GO as a NIR photothermal transducer has been debated,[7a] prompting investigation of rGO, as a 2D nanomaterial with potentially improved NIR absorbance.[7a] Unfortunately, rGO is hydrophobic,[12] and thus requires complex surface modifications to be useful in aqueous environments.[7]

As an alternative to the aforementioned materials, we report the NIR-photothermal properties of chemically exfoliated MoS$_2$ (ceMoS$_2$). ceMoS$_2$ is a mixed phase, two-dimensional amphiphile that is easy to synthesize in large batches and is directly dispersible in water.[13] Further, the magnitude of its ζ potential (-45 mV, comparable to GO)[14] provides great colloidal stability in aqueous media. We show that owing to an absorbance profile reaching into the NIR, ceMoS$_2$ heats up rapidly upon NIR irradiation. Because of its high surface-area-to-mass ratio, ceMoS$_2$ also possesses loading capacities on par with GO, the current best-in-class.[15] Clearly, ceMoS$_2$ possesses many desirable traits present in the aforementioned photothermal agents.

To synthesize ceMoS$_2$, we use the Morrison method[13a,c] which breaks the weak interlayer forces in bulk MoS$_2$ through ultrasonication and the formation of H$_2$ gas. Compared to mechanical exfoliation[16] or vapor-deposited films on wafer templates,[17] the MoS$_2$ sheets obtained through this method tend to lack the crystallinity required for usage as semiconducting active layers.[13c, 18] However, this method renders the resulting sheets water dispersible (they are natively hydrophobic), is scalable, and can be readily adapted for other transition metal dichalcogenides.[13c, 19] A typical synthesis produces approximately 300 mL of MoS$_2$ at a concentration ≥ 300 ppm (see the Experimental Section) and is easily scalable. Physical characterization of the resultant sheets using atomic force microscopy ($n = 100$) revealed mean longest diagonals of 0.80 μm with an average thickness of 1.56 nm ($n = 40$ sheets), which is consistent with a MoS$_2$

[*] Dr. B. Kaehr, Prof. C. J. Brinker
Advanced Materials Laboratory Sandia National Laboratories
Albuquerque, NM 87106 (USA)
and
Department of Chemical and
Nuclear Engineering Center for Micro-engineered Materials
University of New Mexico, Albuquerque, NM 87106 (USA)
E-mail: bjkaehr@sandia.gov

S. S. Chou, J. Kim, B. M. Foley, Dr. M. De, Prof. J. Huang,
Prof. V. P. Dravid
Department of Materials Science and Engineering
International Institute of Nanotechnology
Northwestern University, Evanston, IL 60208 (USA)
E-mail: s-chou@northwestern.edu

Prof. P. E. Hopkins
Department of Mechanical and Aerospace Engineering
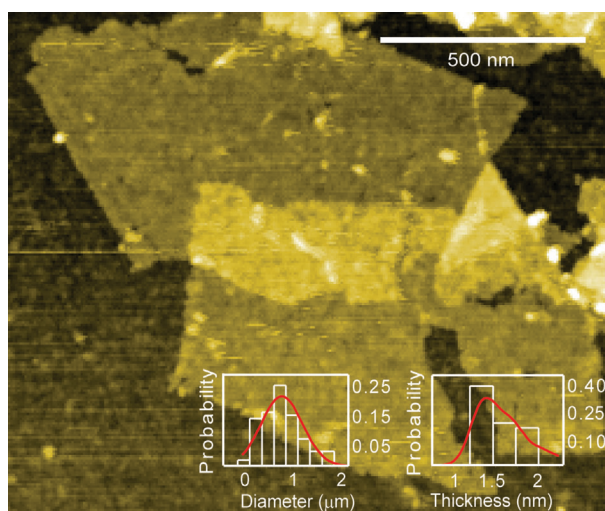University of Virginia, Charlottesville, VA 22904 (USA)

Figure 1. Atomic force microscopy (AFM) micrograph of ceMoS₂ sheets. The insets show diameter and thickness profiles.

monolayer[20] (Figure 1 and Figure S1 in the Supporting Information).

NIR absorbance by ceMoS₂ was then characterized (Figure 2a). Here, the concentration of ceMoS₂ was determined using induction-coupled plasma mass spectroscopy (ICP-MS), which provides parts-per-billion sensitivity (ppb). This enabled the accurate quantification of the ceMoS₂ mass extinction coefficient ($\lambda = 800$ nm, 29.2 L g^{-1} cm^{-1}), which represents a ≈ 7.8-fold increase compared to nano-GO (3.6 L g^{-1} cm^{-1}) and is comparable to nano-rGO (24.6 L g^{-1} cm^{-1}).[7a] It also represents a two times increase over gold nanorods (13.9 L g^{-1} cm^{-1}).[7a]

Next, we investigated photothermal heating of solutions of ceMoS₂, prepared over a range of concentrations, by irradiation with a continuous wave laser at $\lambda = 800$ nm (0.8 W cm^{-2}) and measurement of the solution temperature as a function of time (Figure 2b.). Here, the superior NIR photothermal transduction by ceMoS₂ is demonstrated, as we observed solution temperatures above 40°C, the figure of merit for thermal ablation therapy,[21] to be generated with very low concentrations of ceMoS₂ (< 38 ppm). This is a marked improvement over GO.[7a] Thus, ceMoS₂ combines the NIR heating features of rGO,[7a] with the water dispersibility of GO using a simple and readily scalable batch process. Additionally, x-ray photoelectron spectroscopy (XPS) showed no significant oxidation of as prepared and IR-irradiated ceMoS₂ (Figure S2).

To show that ceMoS₂, in the absence of NIR irradiation, is otherwise biocompatible, we examined its capability to form non-denaturing host–guest interactions with α-chymotrypsin (ChT), a serine protease. Here, ChT was chosen for its broad bio-sensing applicability and its well documented loading capacity in a wide variety of materials, including gold nanoparticles,[22] polymeric micelles,[23] dendrimers,[24] porphyrins,[25] carbon nanotubes,[26] and GO.[14a, 15] As ChT contains a cationic active site that can complex with anionic materials through electrostatic complementation, its loading can be quantified by monitoring enzymatic inhibition by ceMoS₂. To investigate ChT loading on ceMoS₂, we incubated a range of concentrations of ceMoS₂ with 16 μM ChT in 96 well plates. After 30 minutes of incubation, N-succinyl-l-phenylalanine-p-nitroanilide (SPNA), a chromogenic substrate for measuring ChT activity, was added to a final concentration of 2 mM. The data were then fitted using nonlinear regression. From the resulting inhibition curve (Figure 3a), it can be seen that 50% of ChT is inhibited by 5 ppm of ceMoS₂. Full inhibition ($> 95\%$) is attained at 11 ppm. This value is significant, as it demonstrates that ceMoS₂ has a ChT dose-inhibition capacity comparable to GO, which is the current benchmark material (full comparison in the Supporting Information).[15]
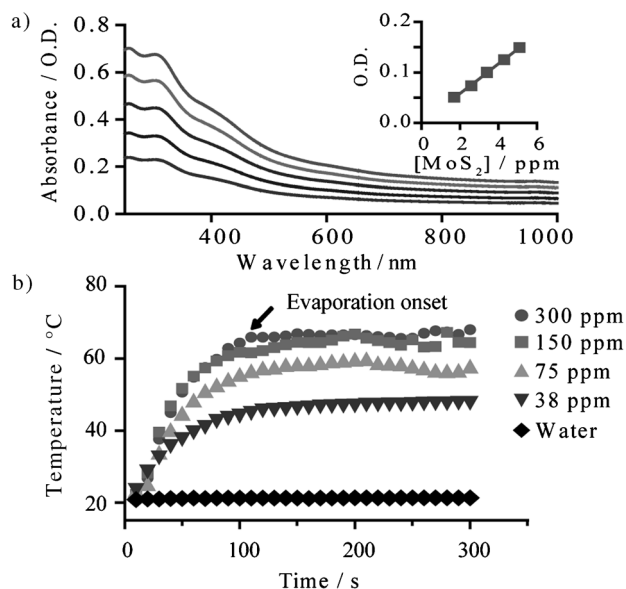

Figure 2. a) Absorbance profile of ceMoS₂. The top curve is 5 ppm. Each subsequent curve is 0.5 times diluted. The inset is the Beer's law plot at 800 nm (O.D. = optical density). b) Photothermal heating curves of ceMoS₂ across a range of concentrations.
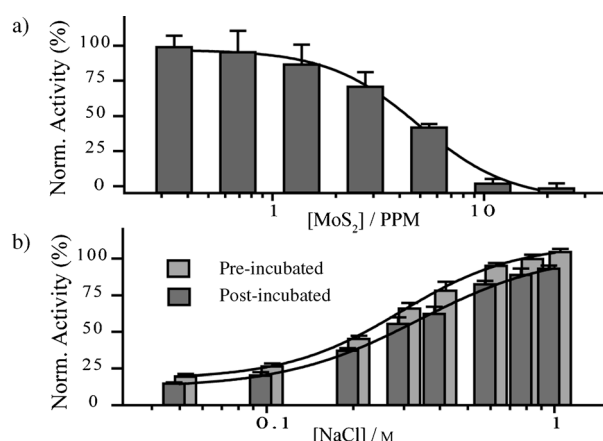

Figure 3. a) Inhibition of ChT using increasing doses of ceMoS₂. b) Activity of ChT–ceMoS₂ pre-incubated and post-incubated with increasing concentrations of NaCl.

To show that the host–guest interaction between ChT and ceMoS₂ is reversible, we incubated ChT with 11 ppm of ceMoS₂ (full inhibition concentration) in media of increasing ionic strength to negate electrostatic interactions.[27] In one set of experiments, ceMoS₂ was added to ChT in media pre-spiked with NaCl (pre-incubated). In another set of experiments, NaCl was added after first allowing ceMoS₂ and ChT to form a complex for 30 minutes (post-incubated). In the case of pre-incubation with NaCl, 100% of ChT activity was observed to be recovered at [NaCl] = 750 mM. Comparatively, only 90% of ChT activity was recovered if NaCl was added after ceMoS₂ was allowed to first form a complex with ChT (Figure 3b). Interestingly, the rate of recovery did not change with increased pre-incubation times (24 h, see the Supporting Information). These observations suggest that either some part of ChT is denatured following complexation with ceMoS₂, or that there may be a two component complexation process where one component acts through non-electrostatic forces.[15]

To distinguish between these mechanisms, we investigated the protein structure of ChT after complexation with ceMoS₂ using circular dichroism (CD) and fluorescence spectroscopy. Here, using CD, it can be seen that native ChT structure presents characteristic minima at 232 and 204 nm (Figure 4a and Figure S3).[15] Upon denaturation (DChT), the minimum at 232 nm diminishes and the minimum at 204 nm intensifies and shifts toward 198 nm (Figure S3). It can also be seen that ChT, once inhibited by complexation with ceMoS₂, displays identical CD spectra to free ChT (Figure 4a). In fact, the CD spectra of ChT remained consistent even after 24 h of incubation with ceMoS₂, thus indicating complexation does not lead to protein denaturation.

The preservation of the ChT structure was also corroborated by fluorescence spectroscopy. Here, as the secondary structure of ChT unravels, its tryptophan (trp) residue becomes increasingly exposed to water. This causes a red-shift in its fluorescence peak, from 334 to 352 nm (Figure S3).[28] As this shift was not observed with the inhibited

ChT–ceMoS₂, the fluorescence spectroscopy data corroborates the findings of the CD study (Figure 4b). It is therefore likely that the 90% recovery seen for ceMoS₂-complexed ChT post-incubated with NaCl is due to a two-component binding process, with the majority due to electrostatic complementarity, and the remaining (non-recovered) binding due to weak intermolecular forces[15,22] attributable to the amphiphillic properties of ceMoS₂.[13b]

The combination of biomolecular friendliness, high protein loading, and favorable photothermal characteristics of ceMoS₂ suggests its potential as an effective NIR photothermal agent. To demonstrate this potential, we irradiated aliquots of ChT-complexed ceMoS₂ with NIR light for 15 minutes ($\lambda = 800$ nm, 0.8 Wcm⁻²). After treatments, secondary structures of ChT were examined with CD and fluorescence spectroscopy (Figure 4a,b and Figure S3). Residual activity was monitored by spiking samples with NaCl (750 mM) and reversing the ChT–ceMoS₂ complexation. The activity of ChT after various treatments is shown in Figure 4c.

In these experiments, it can be seen that the ChT–ceMoS₂ complexes irradiated with NIR laser light showed complete denaturation (Figure 4a,b and Figure S3). Further, they show little enzymatic activity (Figure 4c). This demonstrates ceMoS₂ as an effective enzymatic receptor capable of selective destruction of its targets through NIR photothermal transduction.

To demonstrate the photothermal ablation therapy for mammalian cells, we then examined its administration in vitro. Here, we collected Hela cells at a concentration of 10^5 mL⁻¹. The solution was then spiked with ceMoS₂ to final concentrations of 20 and 40 ppm. These dosages are roughly an order of magnitude lower than those reported in previous GO studies.[6b,29] As with ChT experiments, parallel aliquots were used for controls. All experiments were performed in independent triplicates. After various treatments (irradiated, non-irradiated, with and without ceMoS₂), cells were washed with phosphate-buffered saline (PBS; three times) and then incubated in a 96 well plate for 24 hrs (10 000/well). Cell viabilities were then measured using Cellter 96 (Promega), a negatively charged, water-soluble MTT agent that does not interfere with cell activity measurements.[12]

As shown in Figure 5, cells treated with ceMoS₂ and NIR irradiation ($\lambda = 800$ nm, 20 minutes) show zero viability at both ceMoS₂ concentrations. This is not surprising as solution temperatures reached 57 and 64°C, respectively, well above thermal ablation thresholds. Optical micrographs of the treated cells confirm the Cellter results (Figure S4). This
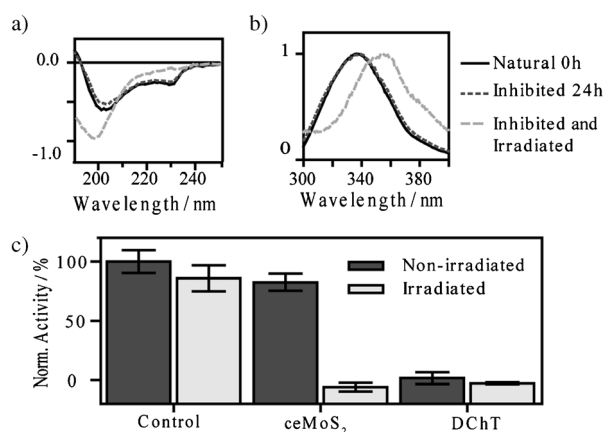

Figure 4. a) Normalized CD and b) fluorescent spectra of select ChT samples after various treatments. A full set of samples is available in the Supporting Information (Norm. = normalized intensity). c) Normalized activity assay of ceMoS₂-ChT or decoupled ChT in 750 mM NaCl after various treatments.
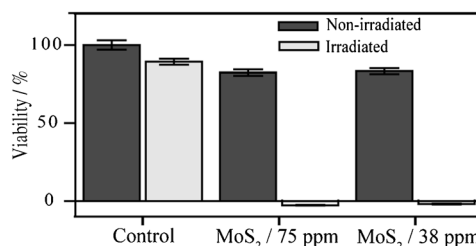

Figure 5. Hela cell viabilities after various treatments.

presents a stark contrast to cells treated with ceMoS$_2$ without irradiation. There, cell viabilities of 82 and 81% were observed. It is thus consistent with previous reports showing MoS$_2$ materials to be relatively non-toxic to cells.[30] Cells irradiated with NIR without ceMoS$_2$ showed a viability of 89%. This observation shows that the photothermal process of ceMoS$_2$ can be extended for cellular destruction.

As the cellular viability is closely related to the temperature rise induced from the ceMoS$_2$ photothermal transduction, we examined the physical processes driving the temperature rise in the cellular matrix by measuring the rate of heat transfer from the ceMoS$_2$ into an aqueous medium with time-domain thermo-transmission (TDTT).[31] TDTT has been used previously by several groups to quantify the thermal boundary conductance[32] between nanosystems suspended in elastically softer media.[31,33] In short, TDTT uses a brief laser pulse to heat the optically absorbing ceMoS$_2$ while a time-delayed probe pulse monitors the temperature change of the ceMoS$_2$. The thermal decay of the ceMoS$_2$ over several nanoseconds is related to the heat flow from the ceMoS$_2$ to the surrounding media, as described in detail elsewhere.[34,35] For our specific TDTT experiments, we measured the thermal decay of 30 ppm of ceMoS$_2$ suspended in deionized water. We monitored the temperature decay at 800 nm to directly mimic the previously described experiments and find the thermal boundary conductance from the ceMoS$_2$ to its surrounding to be (77.5 ± 9) MW m^{-2} K^{-1}. To put this into perspective, this is comparable to the interfacial heat transfer between two solids[36] or between carbon nanotubes and water.[31,33b] This relatively low resistance (high conductance) offers an equivalent resistance of about 10 nm of a typical mammalian cell matrix (assuming a cytoplasmic water content of 70%), indicating the high efficacy of thermal coupling between the ceMoS$_2$ and the surrounding media. Using this measured value of thermal boundary conductance, from steady-state heat transfer theory[34,37] we calculate a 30 K temperature rise in the intracellular medium for a 30 ppm ceMoS$_2$ suspensions irradiated at $\lambda = 800$ nm (0.8 W cm^{-2}).

In summary, we have described the optical and photothermal properties of ceMoS$_2$ and report its effectiveness as a NIR photothermal agent. ceMoS$_2$ displays approximately 7.8 times greater absorbance in the NIR relative to GO, with an extinction coefficient at 800 nm of 29.2 L g^{-1} cm^{-1}, which is higher than that of gold nanorods (13.9 L g^{-1} cm^{-1}) and is comparable to rGO (24.6 L g^{-1} cm^{-1}).[7a] Unlike the hydrophobic rGO, however, ceMoS$_2$ is also directly water dispersible after exfoliation, and easily purified (dialysis under water flow). It also possesses an enhanced biomolecular protein loading capacity comparable to GO, the current best-in-class material.[15] These characteristics provide a foundation to explore the use of ceMoS$_2$ for a wide range of biological applications and beyond (e.g., solar paints and coatings), where broad light absorption into the NIR is desirable.

Experimental Section

Synthesis of ceMoS$_2$: Procedures were adapted from Joensen et al.[16] In a nitrogen environment, ≈ 350 mg of MoS$_2$ powder was immersed in ≈ 3.5 mL of *n*-butyllithium (1.6 M in hexane) and stirred for 48 h. Mixture was then filtered over Whatman #41 filter and rinsed with 100 mL of hexane. To the semi-dry mixture, 300 mL of H$_2$O (18.2 MΩ cm at 25°C) was added. The mixture was sonicated for 1 h to achieve exfoliation. The MoS$_2$ nanosheets were then centrifuged and washed with H$_2$O five times. It was then collected and dialyzed against H$_2$O for 5 days. The concentration was determined by ICP-MS.

Additional experimental details are provided in the Supporting Information.

[1] F. F. Jöbsis-vanderVliet, *J. Biomed. Opt.* **1999**, *4*, 392–396.

[2] X. Huang, I. H. El-Sayed, W. Qian, M. A. El-Sayed, *J. Am. Chem. Soc.* **2006**, *128*, 2115–2120.

[3] W. Zhao, J. M. Karp, *Nat. Mater.* **2009**, *8*, 453–454.

[4] S. E. Skrabalak, J. Chen, Y. Sun, X. Lu, L. Au, C. M. Cobley, Y. Xia, *Acc. Chem. Res.* **2008**, *41*, 1587–1595.

[5] J. Xie, J. Y. Lee, D. I. C. Wang, *Chem. Mater.* **2007**, *19*, 2823–2830.

[6] a) B. Tian, C. Wang, S. Zhang, L. Feng, Z. Liu, *ACS Nano* **2011**, *5*, 7000–7009; b) K. Yang, S. Zhang, G. Zhang, X. Sun, S.-T. Lee, Z. Liu, *Nano Lett.* **2010**, *10*, 3318–3323.

[7] a) J. T. Robinson, S. M. Tabakman, Y. Liang, H. Wang, H. Sanchez Casalongue, D. Vinh, H. Dai, *J. Am. Chem. Soc.* **2011**, *133*, 6825–6831; b) K. Yang, J. Wan, S. Zhang, B. Tian, Y. Zhang, Z. Liu, *Biomaterials* **2012**, *33*, 2206–2214.

[8] F. Xia, T. Mueller, Y.-m. Lin, A. Valdes-Garcia, P. Avouris, *Nat. Nanotechnol.* **2009**, *4*, 839–843.

[9] a) H. Chang, Z. Sun, Q. Yuan, F. Ding, X. Tao, F. Yan, Z. Zheng, *Adv. Mater.* **2010**, *22*, 4872–4876; b) B. Chitara, L. S. Panchakarla, S. B. Krupanidhi, C. N. R. Rao, *Adv. Mater.* **2011**, *23*, 5419–5424.

[10] Z. Yin, H. Li, H. Li, L. Jiang, Y. Shi, Y. Sun, G. Lu, Q. Zhang, X. Chen, H. Zhang, *ACS Nano* **2012**, *6*, 74–80.

[11] C. N. R. Rao, H. S. S. R. Matte, K. S. Subrahmanyam, *Acc. Chem. Res.* **2013**, *46*, 149–159.

[12] K.-H. Liao, Y.-S. Lin, C. W. Macosko, C. L. Haynes, *ACS Appl. Mater. Interfaces* **2011**, *3*, 2607–2615.

[13] a) P. Joensen, R. F. Frindt, S. R. Morrison, *Mater. Res. Bull.* **1986**, *21*, 457–461; b) W. M. R. Divigalpitiya, R. F. Frindt, S. R. Morrison, *Science* **1989**, *246*, 369–371; c) G. Eda, H. Yamaguchi, D. Voiry, T. Fujita, M. Chen, M. Chhowalla, *Nano Lett.* **2011**, *11*, 5111–5116.

[14] a) S. S. Chou, M. De, J. Luo, V. M. Rotello, J. Huang, V. P. Dravid, *J. Am. Chem. Soc.* **2012**, *134*, 16725—16733; b) J. Luo, L. J. Cote, V. C. Tung, A. T. L. Tan, P. E. Goins, J. Wu, J. Huang, *J. Am. Chem. Soc.* **2010**, *132*, 17667–17669.

[15] M. De, S. S. Chou, V. P. Dravid, *J. Am. Chem. Soc.* **2011**, *133*, 17524–17527.

[16] a) B. Radisavljevic, A. Radenovic, J. Brivio, V. Giacometti, A. Kis, *Nat. Nanotechnol.* **2011**, *6*, 147–150; b) H. S. S. Ramakrishna Matte, A. Gomathi, A. K. Manna, D. J. Late, R. Datta, S. K. Pati, C. N. R. Rao, *Angew. Chem.* **2010**, *122*, 4153–4156; *Angew. Chem. Int. Ed.* **2010**, *49*, 4059–4062.

[17] a) K.-K. Liu, W. Zhang, Y.-H. Lee, Y.-C. Lin, M.-T. Chang, C.-Y. Su, C.-S. Chang, H. Li, Y. Shi, H. Zhang, C.-S. Lai, L.-J. Li, *Nano Lett.* **2012**, *12*, 1538–1544; b) Y.-H. Lee, X.-Q. Zhang, W. Zhang,

M.-T. Chang, C.-T. Lin, K.-D. Chang, Y.-C. Yu, J. T.-W. Wang, C.-S. Chang, L.-J. Li, T.-W. Lin, *Adv. Mater.* **2012**, *24*, 2320–2325.

[18] P. Joensen, E. D. Crozier, N. Alberding, R. F. Frindt, *J. Phys. C* **1987**, *20*, 4043.

[19] Z. Zeng, Z. Yin, X. Huang, H. Li, Q. He, G. Lu, F. Boey, H. Zhang, *Angew. Chem.* **2011**, *123*, 11289–11293; *Angew. Chem. Int. Ed.* **2011**, *50*, 11093–11097.

[20] D. J. Late, B. Liu, H. S. S. R. Matte, C. N. R. Rao, V. P. Dravid, *Adv. Funct. Mater.* **2012**, *22*, 1894–1905.

[21] a) H.-C. Huang, K. Rege, J. J. Heys, *ACS Nano* **2010**, *4*, 2892–2900; b) X. Huang, P. K. Jain, I. H. El-Sayed, M. A. El-Sayed, *Photochem. Photobiol.* **2006**, *82*, 412–417; c) J. Overgaard, *Int. J. Radiat. Oncol. Biol. Phys.* **1989**, *16*, 535–549.

[22] N. O. Fischer, C. M. McIntosh, J. M. Simard, V. M. Rotello, *Proc. Natl. Acad. Sci. USA* **2002**, *99*, 5018–5023.

[23] B. S. Sandanaraj, D. R. Vutukuri, J. M. Simard, A. Klaikherd, R. Hong, V. M. Rotello, S. Thayumanavan, *J. Am. Chem. Soc.* **2005**, *127*, 10693–10698.

[24] F. Chiba, T.-C. Hu, L. J. Twyman, M. Wagstaff, *Chem. Commun.* **2008**, 4351–4353.

[25] K. Kano, Y. Ishida, *Chem. Asian J.* **2008**, *3*, 678–686.

[26] B. Zhang, Y. Xing, Z. Li, H. Zhou, Q. Mu, B. Yan, *Nano Lett.* **2009**, *9*, 2280–2284.

[27] A. Verma, J. M. Simard, V. M. Rotello, *Langmuir* **2004**, *20*, 4178–4181.

[28] a) A. S. Ladokhin, *Encyclopedia of Analytical Chemistry*, Wiley, Hoboken, **2006**; b) N. O. Fischer, A. Verma, C. M. Goodman, J. M. Simard, V. M. Rotello, *J. Am. Chem. Soc.* **2003**, *125*, 13387–13391.

[29] Note: Value calculated from reference [7b] using the reported dose (20 mg kg^{-1}) by assuming a typical mouse weight of 250 g and a blood volume of 1.5 mL.

[30] H. Wu, R. Yang, B. Song, Q. Han, J. Li, Y. Zhang, Y. Fang, R. Tenne, C. Wang, *ACS Nano* **2011**, *5*, 1276–1281.

[31] S. T. Huxtable, D. G. Cahill, S. Shenogin, L. Xue, R. Ozisik, P. Barone, M. Usrey, M. S. Strano, G. Siddons, M. Shim, P. Keblinski, *Nat. Mater.* **2003**, *2*, 731–734.

[32] E. T. Swartz, R. O. Pohl, *Rev. Mod. Phys.* **1989**, *61*, 605–668.

[33] a) S. T. Huxtable, D. G. Cahill, S. Shenogin, P. Keblinski, *Chem. Phys. Lett.* **2005**, *407*, 129–134; b) S. D. Kang, S. C. Lim, E.-S. Lee, Y. W. Cho, Y.-H. Kim, H.-K. Lyeo, Y. H. Lee, *ACS Nano* **2012**, *6*, 3853–3860.

[34] D. G. Cahill, *Rev. Sci. Instrum.* **2004**, *75*, 5119–5122.

[35] a) P. E. Hopkins, J. R. Serrano, L. M. Phinney, S. P. Kearney, T. W. Grasser, C. T. Harris, *J. Heat Transfer* **2010**, *132*, 081302; b) A. J. Schmidt, X. Chen, G. Chen, *Rev. Sci. Instrum.* **2008**, *79*, 114902.

[36] E. Pop, *Nano Res.* **2010**, *3*, 147–169.

[37] D.-W. Oh, C. Ko, S. Ramanathan, D. G. Cahill, *Appl. Phys. Lett.* **2010**, *96*, 151906.